



# Numerical studies on a ternary AgInTe<sub>2</sub> chalcopyrite thin film solar cell

Arifuzzaman Joy<sup>a</sup>, Ahnaf Tahmid Abir<sup>a</sup>, Bipanko Kumar Mondal<sup>a,b</sup>, Jaker Hossain<sup>a,\*</sup>

<sup>a</sup> Solar Energy Laboratory, Department of Electrical and Electronic Engineering, University of Rajshahi, Rajshahi 6205, Bangladesh

<sup>b</sup> Department of Electrical & Electronic Engineering, Pundra University of Science & Technology, Bogura, Bogura 5800, Bangladesh

## ARTICLE INFO

### Keywords:

AgInTe<sub>2</sub>  
AlSb  
BaSi<sub>2</sub>  
Thin film solar cell  
SCAPS-1D

## ABSTRACT

This paper theoretically outlines a new *n*-AlSb/*p*-AgInTe<sub>2</sub>/*p*<sup>+</sup>-BaSi<sub>2</sub> solar cell. The dominance of several factors such as depth, carrier density and defects of every layer on the photovoltaic (PV) outcome has been ascertained applying Solar Cell Capacitance Simulator (SCAPS)-1D computer-based simulator. The AgInTe<sub>2</sub> (AIT) solar cell has been probed for finding the role of BaSi<sub>2</sub> as a back surface field (BSF) layer. It is revealed that the device power conversion efficiency (PCE) increments from 30% to 34% owing to the use of BaSi<sub>2</sub> semiconducting BSF with V<sub>OC</sub> = 0.90 V, J<sub>SC</sub> = 43.75 mA/cm<sup>2</sup>, FF = 86.42%, respectively. The rippling of the output parameters with respect to the change in series and shunt resistances has also been probed and demonstrated. All the findings reveal the prospect of *n*-AlSb/*p*-AIT/*p*<sup>+</sup>-BaSi<sub>2</sub> dual-heterojunction thin film photovoltaic cell.

## 1. Introduction

Strong demand for renewable energy has grown in recent years and even the most biomass fuel producing countries are intending to use renewable energy to feed their energy hungrieness. Therefore, the world needs high efficiency solar cells as renewable energy sources. Solar fuel can also stand as an alternative to fossil fuel which use diverse photocatalysts in environmentally friendly way [1]. However, the obstacles that are arising in the playground of massive production of high efficiency solar cells are the high production cost, both in terms of manufacturing and recycling end-of-life cells [2]. In addition, there has been difficulty in developing larger sized cells that can be integrated economically into existing solar panel formats. Besides, at low temperature they exhibit deficiency in stability as well as some perovskite solar cells are made of detrimental component such as lead (Pb) [3]. Each of these technical issues has played a role in slowing the market penetration of solar cells. Silicon-based photovoltaic (PV) industries are striving to minimize module fabrication price by commencing a combination of thin wafers along with boosting cell efficiency. To elevate the efficiency the cell, the silicon wafer width has been lessened lower than 100 μm, by virtue of the progress in open circuit voltage (V<sub>OC</sub>) of the PV cell with a finite Auger recombination [4–8]. In the year of 2017, Kaneka Corporation has manifested a highly efficient silicon heterojunction (HJ) photovoltaic cell with a record PCE of 26.7% and the research has opened a new path in the area of solar photovoltaic cell [9]. However, the theoretical efficiency limit for a single-heterojunction solar cell is 29.4% and this efficiency is just above 2.7% from that reported by Kaneka [10]. Therefore, emergency of a novel method has arisen as this is very close to the performance limit.

\* Corresponding author.

E-mail address: [jak\\_appee@ru.ac.bd](mailto:jak_appee@ru.ac.bd) (J. Hossain).

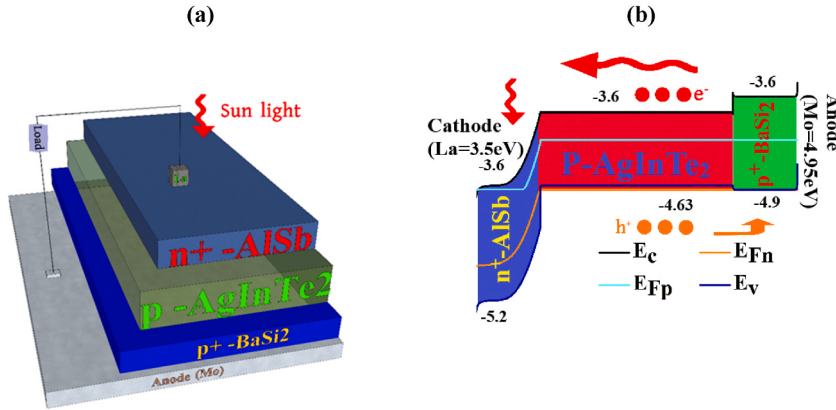


**Fig. 1.** The (a) Designed architecture, (b) electronic energy diagram of  $n\text{-AlSb}/p\text{-AgInTe}_2/p^+\text{-BaSi}_2$  thin film solar cell.

Dual-heterojunction (DH) solar cells have been proposed so that the efficiency of solar cells could be ameliorated [11]. In case of dual-heterojunction solar cell, the Shockley–Queisser (SQ) efficiency boundary is 42–46% [12,13]. Therefore, there is a scope for the efficiency enhancement through DH structure.

Herein, a ternary alloy AgInTe<sub>2</sub>-based thin film solar cell has been studied for high efficiency. AgInTe<sub>2</sub> (AIT) is one of the I-III-VI<sub>2</sub> triune chalcopyrite mixture which has got a special animus because of its application to photovoltaic solar cells and optical devices [14, 15]. Some researchers have focused on AgInTe<sub>2</sub> and the majority of which belongs to elastic constants and specific heat [16]. However, only a few papers have presented the optical and electrical properties of AIT [17]. The AIT has a straight bandgap and it is at the  $\Gamma$  point [18–21], moreover, the density of states (DOS) is steep, which leads to a large Seebeck coefficient [22]. For this reason, AgInTe<sub>2</sub> may be proved as a p-type thermoelectric materials with a doping in the range of  $10^{19}\text{--}10^{20}\text{ cm}^{-3}$ . The thermoelectric transport characteristic confides both on the temperature and on the doping concentration [23].

AgInTe<sub>2</sub> is really novel in the field of photovoltaics and has been used as the absorber layer only in a few works. So far, a couple of reports reveal AIT solar cell with AgInTe<sub>2</sub>/In<sub>2</sub>S<sub>3</sub>/TiO<sub>2</sub>/FTO structure where AIT has been deposited by printing and RF sputtering deposition methods and Au has been used as an electrode [24,25]. The efficiency has been reported in the range of 0.5–1.13%. The efficiency is low mainly due to the lower  $V_{OC}$  and FF which may results from the inappropriate choice of window layer and also deposition method plays important role in high quality film deposition. However, AIT is capable to prove itself as a perfect absorber layer because of obtaining some quality of an ideal absorption layer, for an instance, enriched crystallographic properties, suitable carrier lifetime, exalted optical absorption coefficient and lofty mobility [26].

In addition, a window layer or buffer layer is a layer which stands just over the absorber layer and doped with the opposite conductive material. The window layer is generally used to build a pn junction in a heterojunction thin film solar cell with the absorber layer [27]. An exalted bandgap, pony thickness, and humble series resistance are expected with the window layer for aerial optical throughput. In the composition of a solar cell, window layer material provides a fateful job to enhance the efficiency of a solar cell [28]. Aluminium antimonide (AlSb) could be a spanking option as a window layer in AIT-based thin film solar cell. AlSb is a part of group III-V material having a bandgap of 1.6 eV at a temperature of 300 K [29]. Moreover, AlSb has some other features to choose it as the window material, such as its high melting and boiling point of 1330 and 2740 K, respectively. The most important parameter of AlSb is its index of refraction of 3.3 at 200 nm wavelength, and dielectric constant is 10.9 at radiowave frequencies [30]. Moreover, various technics are available for the deposition of AlSb thin films for an instance hot wall epitaxy, co-evaporation and co-sputtering etc. [31]. However, AlSb has yet not been used with AgInTe<sub>2</sub> based solar cell.

The back surface field (BSF) is a heavily doped layer with a doping of the same type as that of the absorber layer to obtain the pp<sup>+</sup> structure. With the help of BSF layer, it is possible to enlarge the short circuit current, the spectral response and the curtailment of contract resistance. Due to the difference between the doping level of the absorber and BSF layers, a potential barrier is generated which try to incarcerate the minority carriers in the absorber layer [32]. Barium Silicide (BaSi<sub>2</sub>) has been used as a BSF layer in this AIT-based thin film solar cell. BaSi<sub>2</sub> is a sanguine material for enormously efficient thin-film heterostructure solar cell [33]. BaSi<sub>2</sub> is likeable in photovoltaic application for its lofty durability and bandgap of approximately 1.1–1.35 eV [34]. There is an affluence of both Ba and Si in the earth, as a result the BaSi<sub>2</sub> can be used to make a cheap dual-heterojunction solar cell [35]. BaSi<sub>2</sub> is fabricated with the high purity Ge (HPGe) thin film fabrication technique, Vapor phase epitaxy (VPE) technique, molecular beam epitaxy (MBE) technique, solid phase epitaxy (SPE) technique etc. [36–39]. Besides, there is another method called magnetron sputtering method (MSM) which is held on the radio frequency (RF) for developing polycrystalline BaSi<sub>2</sub> films at a subordinate cost on glass substrate [40]. The most exciting characteristics for which BaSi<sub>2</sub> can be used as the BSF layer are the high absorption coefficient of about  $3 \times 10^5\text{ cm}^{-1}$ , a standard indirect bandgap, the diffusion distance of 10  $\mu\text{m}$ , and the minority carrier lifetime of 14  $\mu\text{s}$  [41]. However, as far as we know, there are no records available depicting the usage of BaSi<sub>2</sub> as the BSF layer with AIT-based solar cell.

In this endeavor, we present a novel AIT-based double-heterojunction (DH) thin film photovoltaic cell. Herein, AlSb, AgInTe<sub>2</sub> and BaSi<sub>2</sub> have been utilized as the n-window, p-absorber and p<sup>+</sup>-BSF layers, respectively. The  $n\text{-AlSb}/p\text{-AgInTe}_2/p^+\text{-BaSi}_2$  devices have been evaluated to get superior output Photovoltaic (PV) performances with computational simulations. The quantum efficiency (QE)

**Table 1**

The various parameters of AlSb, AIT and BaSi<sub>2</sub> layers put in the calculation of *n*-AlSb/*p*-AIT/*p*<sup>+</sup>-BaSi<sub>2</sub> thin film solar cell.

Parameters	<i>n</i> -AlSb [42,43]	<i>p</i> -AgInTe <sub>2</sub> [44,45]	<i>p</i> <sup>+</sup> -BaSi <sub>2</sub> [46,47]
Bandgap (eV)	1.6	1.03	1.30
Electron affinity	3.6	3.6	3.3
Thickness ( $\mu\text{m}$ )	0.2	0.6	0.2
Dielectric permittivity (relative)	12.04	8.9	10
Effective DOS at CB ( $\text{cm}^{-3}$ )	$7.8 \times 10^{17}$	$3.66 \times 10^{19}$	$1.0 \times 10^{19}$
Effective DOS at VB ( $\text{cm}^{-3}$ )	$1.8 \times 10^{19}$	$1.35 \times 10^{19}$	$1.0 \times 10^{19}$
Electron thermal velocity (cm/s)	$1.7 \times 10^7$	$1.0 \times 10^7$	$1.0 \times 10^7$
Hole thermal velocity (cm/s)	$1.4 \times 10^7$	$1.0 \times 10^7$	$1.0 \times 10^7$
Hole mobility ( $\text{cm}^2/\text{vs}$ )	$4.2 \times 10^2$	$8.870 \times 10^2$	$2.0 \times 10^1$
Electron mobility ( $\text{cm}^2/\text{vs}$ )	$2 \times 10^2$	$1.011 \times 10^3$	$2.0 \times 10^1$
Shallow uniform donor density, N <sub>D</sub> ( $\text{cm}^{-3}$ )	$1 \times 10^{17}$	0	0
Shallow uniform acceptor density, N <sub>A</sub> ( $\text{cm}^{-3}$ )	0	$1.0 \times 10^{20}$	$1.0 \times 10^{20}$
Bulk defects ( $\text{cm}^{-3}$ )	$1 \times 10^{14}$	$1 \times 10^{13}$	$1 \times 10^{14}$
Defects at various interfaces:			
Heterointerfaces			Defect density ( $\text{cm}^{-2}$ )
<i>n</i> <sup>+</sup> -AlSb/ <i>p</i> -AgInTe <sub>2</sub>			$1.00 \times 10^{10}$
<i>p</i> -AgInTe <sub>2</sub> / <i>p</i> <sup>+</sup> -BaSi <sub>2</sub>			$1.00 \times 10^{10}$

of the photovoltaic device has also been enumerated and delimitated in niceties with output photovoltaic parameters such as J<sub>SC</sub>, V<sub>OC</sub>, FF and efficiency. This work premises that the AIT-based solar cell with AlSb as window and BaSi<sub>2</sub> as BSF may get high importance in the upcoming days.

## 2. Device architecture and numerical computation

Fig. 1(a) delimitates the schematic diagram of the presented AgInTe<sub>2</sub> chalcopyrite-based dual-heterojunction solar cell and the energy band diagram is delineated in Fig. 1(b). AgInTe<sub>2</sub> is a *p*-type material with an optical bandgap of 1.03 eV, electron affinity of 3.6 eV, and ionization energy of 4.63 eV which has been used as a solar absorber layer. It is capable to form a pn heterojunction with the *n*-type AlSb material, which has a bandgap of 1.6 eV and an electron affinity of 3.6 eV. With these identical values, they form a suitable *n*-AlSb/*p*-AgInTe<sub>2</sub> heterojunction. On the opposite side, the BaSi<sub>2</sub> which has seized a bandgap of 1.3 eV and electron affinity of 3.3 eV is susceptible to form a pp<sup>+</sup> heterojunction with AgInTe<sub>2</sub> material. So, three of them in association have made a congruous *n*-AlSb/*p*-AIT/*p*<sup>+</sup>-BaSi<sub>2</sub> heterojunction solar cell. The light enters the cell through the *n*-AlSb window layer of the device. Moreover, Lanthanum with a work function of 3.5 eV and molybdenum with a work function of 4.95 eV have been utilized as the hindmost and foremost contract, respectively for efficient charge collection.

The proposed device structure was simulated by SCAPS 1D simulator (version 3.3.07), delivered from Professor M. Burgelman and his group, University of Gent, Belgium, which essentially resolves Poisson's equations of continuity for holes and electrons. The simulation was done under 1 sun irradiation with a power density of 100 mW/cm<sup>2</sup> of global air mass (AM) of 1.5G spectrum. The absorption coefficient data for the AgInTe<sub>2</sub> absorber, the BaSi<sub>2</sub> BSF, and the AlSb window layer were assigned from the SCAPS traditional E<sub>g</sub>-sqrt model with default values. Defects have a significant impact on how well a solar cell performs. In the simulation, donor/acceptor/acceptor type of defects were set for window/absorber/BSF layer, respectively. Gaussian shaped energetic distribution was used for the defects in all layers with default capture cross-section for electrons and holes. This simulation avoided radiative recombination and auger recombination as large number of bulk defects were considered. The surface-recombination velocity of electron/hole that affects the quantum efficiency and reverse saturation current was set to  $10^5/10^7$  cm/s for the front and  $10^7/10^5$  cm/s for back metallic contacts. The physical parameters of different layers were taken from reported works as shown in Table 1.

## 3. Results and discussion

The output parameters of a photovoltaic (PV) cell for example short circuit current density (J<sub>SC</sub>), open circuit voltage (V<sub>OC</sub>), fill factor (FF), and efficiency ( $\eta$ ) vary with the thicknesses of different layers, for an instance the window, absorber, and back surface field (BSF) layer, and with the carrier concentration and defect density of those layers. The performance parameters also vary with the shunt and series resistances, which depend on temperature. The maximum output of the AIT solar cell has been found from optimizing the device structure.

### 3.1. Device outcome with AIT absorber layer

In this part, the influences of AIT semiconducting layer on PV parameters of *n*-AlSb/*p*-AgInTe<sub>2</sub>/*p*<sup>+</sup>-BaSi<sub>2</sub> solar cell have been studied. The depth, doping density, and defect density of the absorber layer have been varied from 0.25 to 1.5  $\mu\text{m}$ ,  $1 \times 10^{17}$  to  $1 \times 10^{22}$  cm<sup>-3</sup>, and  $1 \times 10^{11}$  to  $1 \times 10^{16}$  cm<sup>-3</sup>, respectively. The width, doping concentration, and volume defects of the window and the back surface field layers have been kept fixed as shown in Table 1.

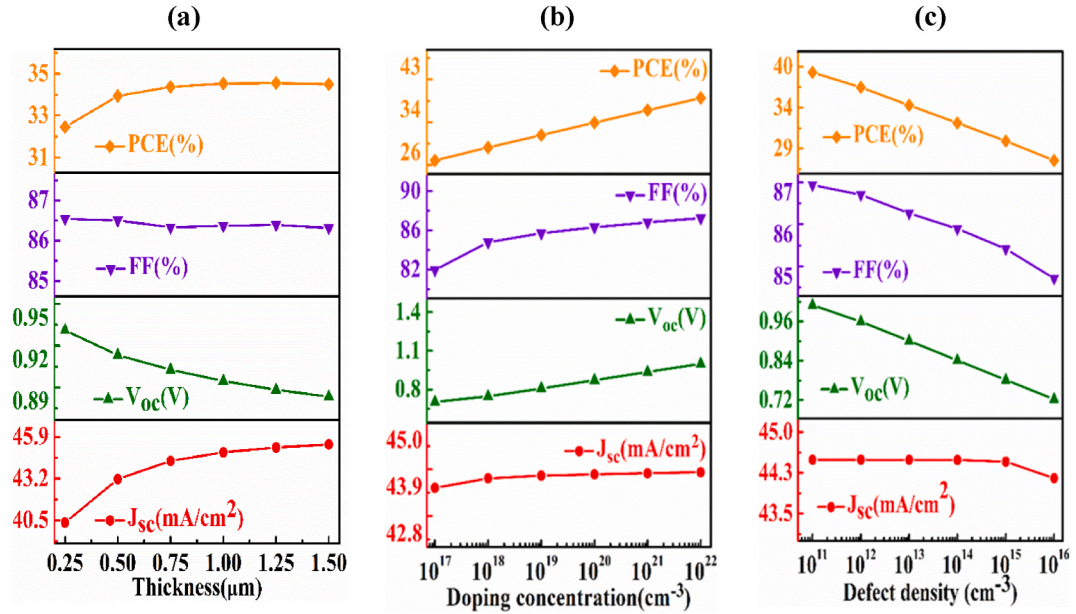


**Fig. 2.** The fluctuation of output performance parameters ( $V_{\text{oc}}$ ,  $J_{\text{sc}}$ , FF,  $\eta$ ) of  $n\text{-AlSb}/p\text{-AgInTe}_2/p^+\text{-BaSi}_2$  photovoltaic cell as a function of (a) thickness, (b) carrier and (c) defects of AgInTe<sub>2</sub> absorber layer.

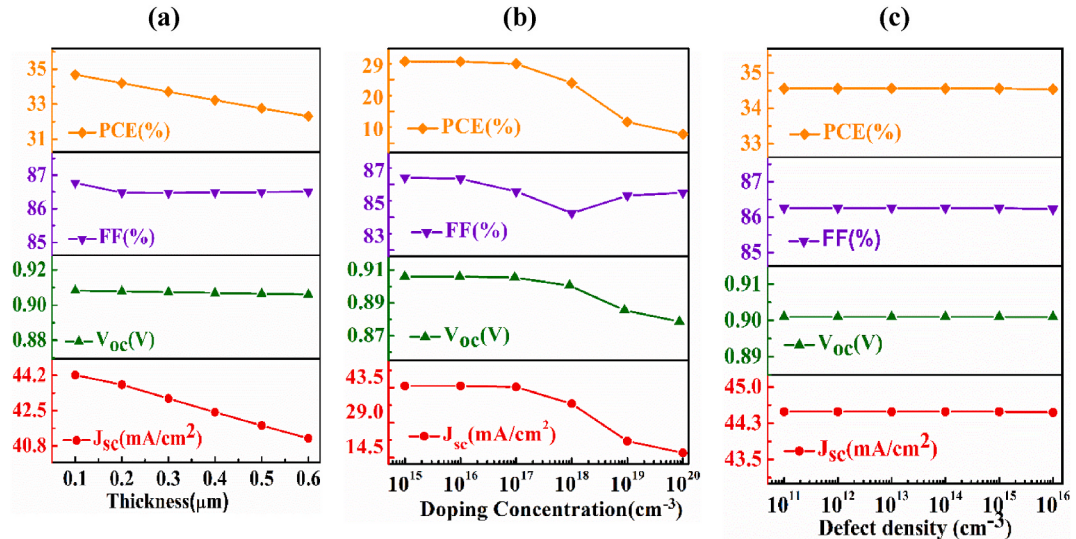


**Fig. 3.** The fluctuation of output performance ( $V_{\text{oc}}$ ,  $J_{\text{sc}}$ , FF,  $\eta$ ) of  $n\text{-AlSb}/p\text{-AIT}/p^+\text{-BaSi}_2$  solar PV cell as a function of (a) thickness, (b) carrier density and (c) defects of AlSb window layer.

**Fig. 2(a)** delineates the photovoltaic output parameters of  $n\text{-AlSb}/p\text{-AIT}/p^+\text{-BaSi}_2$  solar cell with varying the breadth of the absorber layer. It is visualized in the figure that both the fill factor and open-circuit voltage decrease with mounting width of the absorber layer and both the short circuit current and efficiency ( $\eta$ ) increase with increasing thickness. The  $J_{\text{sc}}$  and  $\eta$  of the device increase from 40.5 to 45.9  $\text{mA}/\text{cm}^2$  and from 33 to 35%, respectively. The thicker absorber layer enhances the possibility of more light absorption. As a result, more electron and hole pairs are created which enhances the short circuit current [48]. On the opposite site, as the reverse saturation current enhances in accordance to the thickness, there is a negative change on the value of  $V_{\text{OC}}$  from 0.95 to 0.89 V and FF from 87 to 86% [49]. However, the power conversion efficiency (PCE) of the device increases depending on the significant increase of  $J_{\text{sc}}$ .

**Fig. 2(b)** presents the dependence of the photovoltaic parameters of  $n\text{-AlSb}/p\text{-AgInTe}_2/p^+\text{-BaSi}_2$  solar cell on the fluctuation of the doping concentration of the AIT absorber layer. The carrier density of the layer enrolled to absorb photons has a fateful role on the PV parameters. The expression which relates the  $V_{\text{OC}}$  with carrier concentration is  $V_{\text{OC}} = (kT/q) \ln [(N_A + \Delta n) \Delta n / n_i^2]$ , where,  $n_i$  stands for

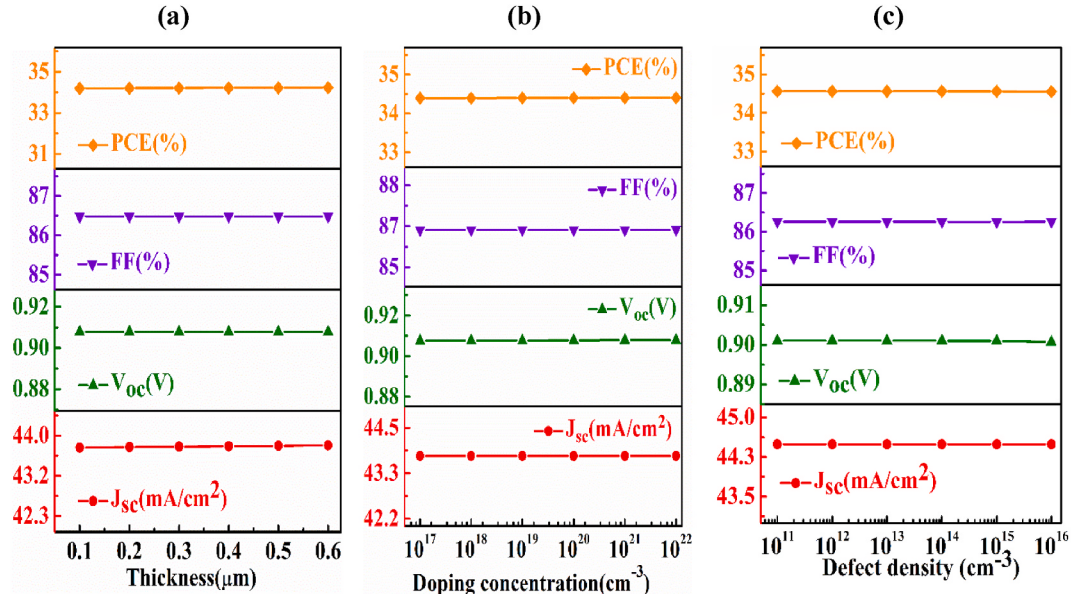


**Fig. 4.** The fluctuation of output performance ( $V_{oc}$ ,  $J_{sc}$ , FF,  $\eta$ ) of  $n$ -AlSb/ $p$ -AgInTe<sub>2</sub>/ $p^+$ -BaSi<sub>2</sub> device as a function of (a) thickness, (b) carrier and (c) defect density of BaSi<sub>2</sub> back surface layer.

intrinsic concentration, doping concentration is denoted by  $N_A$  and excess carrier is denoted by  $\Delta n$  [50]. It can be noticed that all performance parameters increase with increasing carrier in the AIT absorber layer. This is because, with the advancement of doping concentration, the mobility of carrier also increase which leads to increase in short circuit current [51]. Concurrently, the value of  $V_{oc}$  rises from 0.8 to 1 V as with the increment of hole density which results from the rise in built-in voltage with doping. Moreover, there is a crucial change on the value of the fill factor and the efficiency from 82 to 86% and 26% to 34%, respectively. The reason behind this is amelioration of doping concentration degrades the value of series resistance [52].

Fig. 2(c) presents the reliance of the PV output performance of  $n$ -AlSb/ $p$ -AgInTe<sub>2</sub>/ $p^+$ -BaSi<sub>2</sub> photovoltaic cell on the modulation of the defects of the AIT layer. All performance parameters are seen to decline with growing density of defect of the absorber layer except the grade of  $J_{sc}$  which has maintained almost a constant value up to  $10^{15} \text{ cm}^{-3}$ . Beyond this boundary, the value of  $J_{sc}$  depicts a decrement. The grade of  $V_{oc}$ , FF and PCE depict a change from 1 to 0.72 V, 87 to 84.5% and 40 to 29%, respectively. This is because defects can raise the reverse saturation current and decrease the mobility of carriers [53]. The PCE of the device reaches to 40% when defect density is fixed at  $1 \times 10^{11}$  and further increasing of defect density makes down of efficiency.

### 3.2. Device outcome with AlSb window layer

To investigate the dependency of the AlSb window layer, the width, doping concentration, and defect density of the AlSb layer have been altered from 0.1 to 0.6  $\mu\text{m}$ ,  $1 \times 10^{15}$  to  $1 \times 10^{20} \text{ cm}^{-3}$ , and  $1 \times 10^{11}$  to  $1 \times 10^{16} \text{ cm}^{-3}$ , respectively.

Fig. 3(a) delineates the consequence of the variation of the window layer's thickness on the PV parameters of the  $n$ -AlSb/ $p$ -AgInTe<sub>2</sub>/ $p^+$ -BaSi<sub>2</sub> solar cell. The  $J_{sc}$  and PCE are noticed to decrease with the ameliorating of the thickness of the AlSb layer, this is because of the enhancement of parasitic absorption which prevents the photons from having a lower wavelength to approach the absorber layer [54]. The boundary of the alternation of  $J_{sc}$  is from 44 to 40  $\text{mA}/\text{cm}^2$ . The maximum efficiency of 35% is obtained at an initial thickness of 0.1  $\mu\text{m}$ , then it reduces to 31% at 0.6  $\mu\text{m}$  width. On the contrary, the value of  $V_{oc}$  and FF are not affected much by the fluctuation of the width of the window layer. For the reason of high carrier mobility in association with a wide bandgap, the depth of the window layer cannot manipulate the PV parameters strongly [55].

The influence of doping concentration of AlSb window on the PV outcomes of  $n$ -AlSb/ $p$ -AgInTe<sub>2</sub>/ $p^+$ -BaSi<sub>2</sub> solar cell has been depicted in Fig. 3(b). It is seen that the  $J_{sc}$  and efficiency are very sensitive to the doping concentration and their values follow a downward direction. In the studied range of carrier concentration, the  $J_{sc}$  and PCE decrease from 43.5 to 14.5  $\text{mA}/\text{cm}^2$  and from 29 to 10%, respectively, though the  $V_{oc}$  and FF are not so sensitive to the carrier concentration. The increase in free carrier recombination at greater doping concentrations is what has caused the decrease in  $J_{sc}$  and PCE [56].

Fig. 3(c) shows the change in PV performances of the  $n$ -AlSb/ $p$ -AgInTe<sub>2</sub>/ $p^+$ -BaSi<sub>2</sub> device with the defect density of the AlSb layer. It is noted that the defects up to  $10^{16} \text{ cm}^{-3}$  in the AlSb layer have almost no impact on the output PV parameters of the AIT photovoltaic device. However, further increment of defect density increases the dark current which may have a serious influence on device performances [57].

Hence, it can be concluded that the AlSb window layer could be used to control the optical losses and the electrical peculiarity of the  $n$ -AlSb/ $p$ -AIT/ $p^+$ -BaSi<sub>2</sub> thin film PV device.

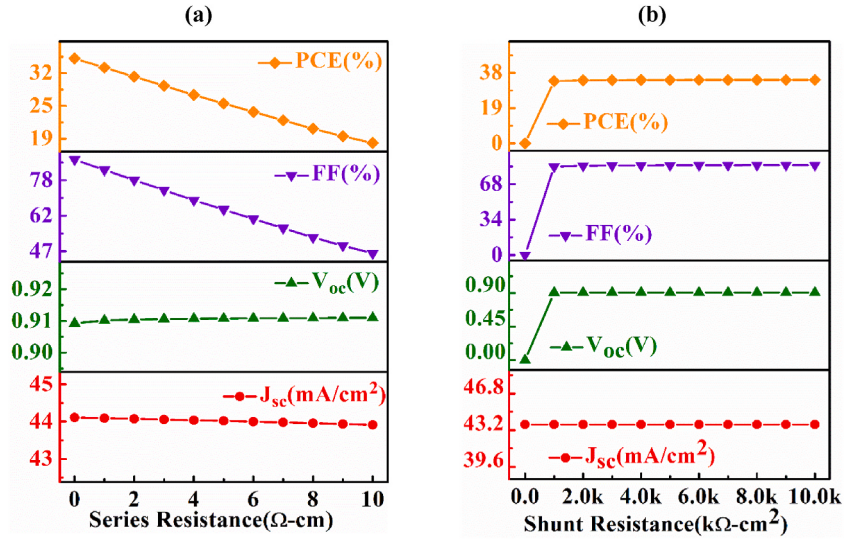


Fig. 5. The impact of (a) series and (b) shunt resistances on  $n$ -AlSb/ $p$ -AgInTe<sub>2</sub>/ $p^+$ -BaSi<sub>2</sub> solar cell.

### 3.3. Device outcome with BaSi<sub>2</sub> back surface field layer

In this part, the effect of BaSi<sub>2</sub> BSF layer on the  $n$ -AlSb/ $p$ -AgInTe<sub>2</sub>/ $p^+$ -BaSi<sub>2</sub> photovoltaic device has been probed in detail. The width, doping density, and defect density of the BaSi<sub>2</sub> BSF layer have been altered from 0.1 to 0.6  $\mu\text{m}$ ,  $1 \times 10^{17}$  to  $1 \times 10^{22} \text{ cm}^{-3}$ , and  $1 \times 10^{11}$  to  $1 \times 10^{16} \text{ cm}^{-3}$ , respectively.

Fig. 4(a) describes the dominance of BSF layer breadth on the photovoltaic outcomes of the  $n$ -AlSb/ $p$ -AgInTe<sub>2</sub>/ $p^+$ -BaSi<sub>2</sub> PV cell and no variations of the output parameters have been found with respect to the alternation of thickness. But, further advancement of thickness of BaSi<sub>2</sub> may have a negative role on the PV parameters. The cause behind this is with the improvement of BSF thickness the series resistance is also enhanced [58].

Fig. 4(b) displays how the PV parameters are related to the alteration of the doping concentration of the BSF layer. No change has been recorded throughout the observed range but it may be predicted that beyond this range there is a slight negation of the PV parameters. The auger recombination may get domination with a higher doping concentration which is harmful to efficiency [59].

Fig. 4(c) imprints the character of the fluctuation of the defects in the BaSi<sub>2</sub> BSF layer on the PV output of the presented solar PV cell. With the improvement of defect density, there is only a weeny change in the performance parameters has been noticed which can be considered to be constant. But the access amount of defects may have advanced the dark current which is dangerous for the activity of the presented solar cell [57].

### 3.4. Impact of resistances on device performance

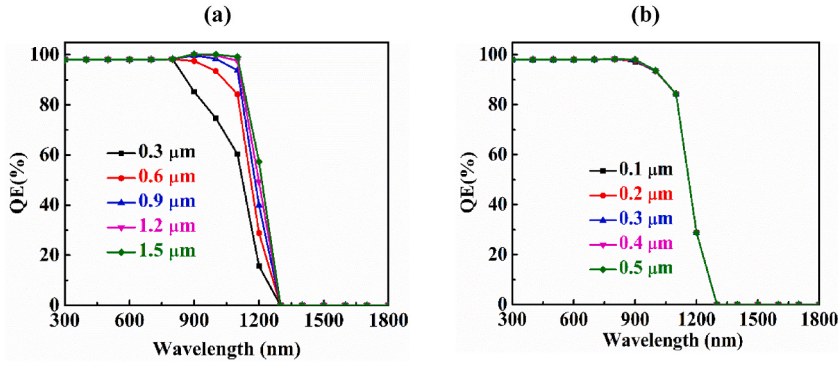
The photovoltaic performance of a cell massively influenced by the series and shunt resistances of the device. The sources of these resistances are the attachment among various active layers, metal connections, and defects related to fabrication [60,61]. The series resistance is liable for causing a drop of voltage across the body of the PV device, whereas the shunt resistance makes a short path in the device for the current when the applied voltage across the cell is zero.

Fig. 5(a) shows the modulation of output parameters with the switching of series resistance. It is perceived that both the  $V_{\text{OC}}$  and  $J_{\text{SC}}$  are less sensitive to the variation of series resistance but both the FF and efficiency are highly sensitive to the change of series resistance. This is because the improvement of series resistance decreases the FF tremendously.

Fig. 5(b) sketches the alteration of output parameters of the  $n$ -AlSb/ $p$ -AgInTe<sub>2</sub>/ $p^+$ -BaSi<sub>2</sub> DH PV device as a function of shunt resistance. Except  $J_{\text{SC}}$ , all the output parameters show a positive change with the improvement of shunt resistance up to a value of  $1.5 \text{ k}\Omega/\text{cm}^2$  and then they stay at a constant value. In other words, with the decrement of the shunt resistance the performance parameters delineate a negative impression. Thus the highest value of PCE should be recorded with the lowest value of series resistance and the highest value of shunt resistance.

### 3.5. QE with and without BaSi<sub>2</sub> BSF layer

The ratio between the total aggregated charges to the quantity of alit photons is denoted as the quantum efficiency (QE) of a photovoltaic cell. We get the maximum QE of 100% when all the incident photons are converted into electric charges. We measure the quantum efficiency as a function of wavelength [53,57]. In Fig. 6(a), the quantum efficiency has been depicted in regard to the fluctuation of wavelength with deferent thicknesses of the absorber layer. This graph shows that the quantum efficiency escalates with



**Fig. 6.** Changing of quantum efficiency as a function of wavelength for (a) AIT absorber and (b) BaSi<sub>2</sub> BSF layer at various thicknesses.

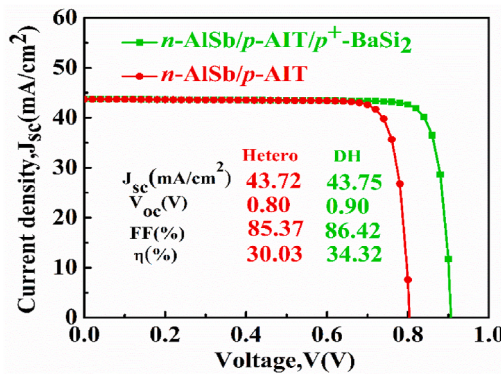


**Fig. 7.** The Current (J)-Voltage (V) characteristics of the AIT solar cell including and excluding BaSi<sub>2</sub> BSF layer.

the rising of the absorber layer thickness. The reason behind this is the absorption of photons enhanced with a wider absorber layer which also makes more electron-hole pairs resulting higher  $J_{SC}$ .

Fig. 6(b) displays the undulation of quantum efficiency with different thickness of the BaSi<sub>2</sub> BSF layer. No variation of quantum efficiency is recorded with the seesaw of the width of the BSF layer just because the thickness of back surface field (BSF) is not creating the barrier for charge carriers. The BSF helps to confine the minority carriers generated at the surface of the PV cell. If the BSF is too thin, the minority carriers will diffuse out of the solar cell before they can be collected by the electrodes. If the BSF is too thick, the minority carriers will have a difficult time reaching the electrodes. The thickness of the BSF is therefore critical to the performance of the solar cell.

### 3.6. Overall output of $n$ -AlSb/ $p$ -AIT/ $p^+$ -BaSi<sub>2</sub> photovoltaic cell

Herein, the contribution of the  $n$ -AlSb/ $p$ -AIT/ $p^+$ -BaSi<sub>2</sub> photovoltaic cell has been analyzed. Fig. 7 shows the current (J)-voltage (V) graphs of the  $n$ -AlSb/ $p$ -AIT heterojunction and  $n$ -AlSb/ $p$ -AIT/ $p^+$ -BaSi<sub>2</sub> double-heterojunction PV devices with fine-tune structures. The optimal thicknesses of AlSb window, AIT absorber and BaSi<sub>2</sub> semiconductors are 0.2, 0.6, and 0.2 μm, orderly. The doping concentration of the same layers are  $10^{17}$ ,  $10^{20}$ , and  $10^{20}$  cm<sup>-3</sup>, accordingly. However, the defect densities are fixed at  $10^{14}$ ,  $10^{13}$  and  $10^{14}$  cm<sup>-3</sup> for window, absorber and BSF layers, respectively. It is visualized from the figure that the  $n$ -AlSb/ $p$ -AIT cell architecture attains output parameters  $J_{SC} = 43.72$  mA/cm<sup>2</sup>,  $V_{OC} = 0.80$  V, FF = 85.37% and efficiency = 30.03%. Whereas, with the inclusion of BaSi<sub>2</sub> layer, the  $n$ -AlSb/ $p$ -AIT heterojunction device turns into  $n$ -AlSb/ $p$ -AIT/ $p^+$ -BaSi<sub>2</sub> PV device and there is an improvement on the output parameters. The improved output parameters are  $J_{SC} = 43.75$  mA/cm<sup>2</sup>,  $V_{OC} = 0.90$  V, FF = 86.42% and efficiency = 34.32%. The  $J_{SC}$  experiences only a meager change as all the alit photons are absorbed in AIT layer before reaching the relatively wide bandgap BaSi<sub>2</sub> BSF layer. However, there is a noticeable rise in the value of  $V_{OC}$  as the cause of the improvement of supreme built-in voltage at the  $n$ -AlSb/ $p$ -AIT and  $p$ -AIT/ $p^+$ -BaSi<sub>2</sub> heterojunctions. An improvement in the efficiency is also noticed and the reason behind this is the advancement of the value of  $V_{OC}$ .

However, in order to validate the potential of BaSi<sub>2</sub> BSF layer, CuInSe<sub>2</sub> semiconductor based CdS/ $p$ -CuInSe<sub>2</sub>/ $p^+$ -BaSi<sub>2</sub> solar cell has been considered. CuInSe<sub>2</sub> (CIS) is an I-III-VI group material like AIT with an optical bandgap of 1.04 eV which is close to that of AIT (1.03 eV) [62]. CIS based ZnO/ $n$ -CdS/ $p$ -CIS with Mo metal as anode shows an experimental efficiency of ~15% with a  $V_{OC}$  of 0.513 V,  $J_{SC} = 40.40$  mA/cm<sup>2</sup> and FF = 71.6% [63]. The same structure has been used in SCAPS that produces an efficiency of 16.39% with  $V_{OC} = 0.526$  V,  $J_{SC} = 39.65$  mA/cm<sup>2</sup>, and FF = 78.58% which is almost consistent with the experimental result. Then, BaSi<sub>2</sub> BSF layer has

been added in the structure with the physical parameters shown in [Table 1](#). The ZnO/n-CdS/p-CIS/p<sup>+</sup>-BaSi<sub>2</sub> device with Mo anode provides a PCE of 21.65% with a V<sub>OC</sub> = 0.624 V, J<sub>SC</sub> = 45.25 mA/cm<sup>2</sup> and FF = 76.06%. Therefore, it can be concluded that as BaSi<sub>2</sub> BSF layer shows potential in CuInSe<sub>2</sub> based ZnO/n-CdS/p-CuInSe<sub>2</sub>/p<sup>+</sup>-BaSi<sub>2</sub> device, it will also have high impact on n-AlSb/p-AlInTe<sub>2</sub>/p<sup>+</sup>-BaSi<sub>2</sub> dual-heterojunction thin film photovoltaic cells.

#### 4. Conclusion

In this effort, we have explored the operation of a photovoltaic device based on AgInTe<sub>2</sub> ternary chalcopyrite semiconducting material. AgInTe<sub>2</sub> as the absorber layer, AlSb as the window layer, and BaSi<sub>2</sub> as the back surface field layer have been chosen for the device structure. Best performance has been attained by taking the absorber width of 0.6 μm, BSF layer thickness of 0.2 μm and the window layer thickness of 0.2 μm. The excellent values of performance parameters which have been obtained are J<sub>SC</sub> = 43.75 mA/cm<sup>2</sup>, V<sub>OC</sub> = 0.90 V, FF = 86.42% and efficiency = 34.32%. Undoubtedly, these numbers are rich in the present days. Further research in this device may attain more fruitful results in future. Hopefully, these outcomes instigate the potential of highly effective AIT-based n-AlSb/p-AlInTe<sub>2</sub>/p<sup>+</sup>-BaSi<sub>2</sub> photovoltaic cell to combat the world energy crisis.

#### Author contribution statement

Arifuzzaman Joy: Ahnaf Tahmid Abir: Jaker Hossain: Conceived and designed the experiments; Performed the experiments; Analyzed and interpreted the data; Contributed reagents, materials, analysis tools or data; Wrote the paper.

Bipanko Kumar Mondal: Analyzed and interpreted the data; Wrote the paper.

#### Data availability statement

Data will be made available on request.

#### Declaration of competing interest

The authors declare that they have no known competing financial interests or personal relationships that could have appeared to influence the work reported in this paper.

#### Acknowledgements

The authors are indebted to Prof. Dr. Marc Burgelman, University of Gent, Belgium, for imparting SCAPS simulation software.

#### Appendix A. Supplementary data

Supplementary data to this article can be found online at [10.1016/j.heliyon.2023.e19011](https://doi.org/10.1016/j.heliyon.2023.e19011).

#### References

- [1] S. Styring, Artificial photosynthesis for solar fuels, *Faraday Discuss* 155 (2012) 357–376.
- [2] T.K. Nideep, M. Ramya, M. Kailasath, An investigation on the photovoltaic performance of quantum dot solar cells sensitized by CdTe, CdSe and CdS having comparable size, *Superlattice. Microst.* 141 (2020), 106477.
- [3] V. Steinmann, R.E. Brandt, T. Buonassisi, Photovoltaics: non-cubic solar cell materials, *Nat. Photonics* 9 (2015) 355–357.
- [4] R.M. Swanson, Developments in Silicon Solar Cells, in: *Proceedings of IEEE Electron Devices Meeting*, Washington, DC, vols. 10–12, December 2007, pp. 359–362. IEEE, 2007.
- [5] D. Sarti, R. Einhaus, Silicon feedstock for the multi-crystalline photovoltaic industry, *Sol. Energy Mater. Sol. Cell.* 72 (2002) 27–40.
- [6] A.G. Aberle, Surface passivation of crystalline silicon solar cells: a review, *Prog. Photovoltaics* 8 (2000) 473–487.
- [7] F. Dross, J. Robbelein, B. Vandevelde, E. Van Kerschaver, I. Gordon, G. Beaucarne, J. Poortman, Stress-induced large-area lift-off of crystalline Si films, *Appl. Phys. A* 89 (2007) 149–152.
- [8] T. Mishima, M. Taguchi, H. Sakata, E. Maruyama, Development status of high-efficiency HIT solar cells, *Sol. Energy Mater. Sol. Cells* 95 (2011) 18–21.
- [9] K. Yoshikawa, H. Kawasaki, W. Yoshida, T. Irie, K. Konishi, K. Nakano, T. Uto, D. Adachi, M. Kanematsu, H. Uzu, K. Yamamoto, Silicon heterojunction solar cell with interdigitated back contacts for a photoconversion efficiency over 26%, *Nat. Energy* 2 (2017), 17032.
- [10] A. Richter, M. Hermle, S.W. Glunz, Reassessment of the limiting efficiency for crystalline silicon solar cells, *IEEE J. Photovoltaics* 3 (2013) 1184–1191.
- [11] I. Almansouri, A. Ho-Baillie, S.P. Bremner, M.A. Green, Supercharging silicon solar cell performance by means of multijunction concept, *IEEE J. Photovoltaics* 5 (2015) 968–976.
- [12] A.D. Vos, Detailed balance limit of the efficiency of tandem solar cells, *J. Phys. D Appl. Phys.* 13 (1980) 839–846.
- [13] A.S. Brown, M.A. Green, Detailed balance limit for the series constrained two terminal tandem solar cell, *Physica E* 14 (2002) 96–100.
- [14] I.V. Bodnar, V.F. Gremenok, K. Bente, Th Doering, W. Schmitz, Optical properties of AgInTe<sub>2</sub> films prepared by pulsed laser deposition, *Phys. Status Solidi A* 175 (1999) 607–613.
- [15] A.S. Verma, Thermal properties of chalcopyrite semiconductors, *Phil. Mag.* 89 (2009) 183–193.
- [16] A.V. Kopytov, A.V. Kosobutsky, Thermodynamic and elastic properties of AgInSe<sub>2</sub> and AgInTe<sub>2</sub>, *Phys. Solid State* 52 (2010) 1359–1361.
- [17] A. Jagomagi, J. Krustok, J. Raudoja, M. Grossberg, I. Oja, M. Krunkus, M. Danilson, Photoluminescence and Raman spectroscopy of polycrystalline AgInTe<sub>2</sub>, *Thin Solid Films* 480–481 (2005) 246–249.

- [18] Y. Zhang, Bandgap nature of chalcopyrite  $ZnXP_2$  ( $X=Si, Ge, Sn$ ), *Comput. Mater. Sci.* 133 (2017) 152–158.
- [19] S. Bagci, B.G. Yalcin, H.A.R. Aliabad, S. Duman, B. Salmankurt, Structural, electronic, optical, vibrational and transport properties of  $CuBX_2$  ( $X = S, Se, Te$ ) chalcoprites, *RSC Adv.* 6 (2016) 59527–59540.
- [20] V.K. Gudelli, V. Kanchana, G. Vaitheswaran,  $CuAlTe_2$ : a promising bulk thermoelectric material, *J. Alloys Compd.* 648 (2015) 958–965.
- [21] S. Sharma, A.S. Verma, R. Bhandari, S. Kumari, V.K. Jindal, Ab initio studies of structural, electronic, optical, elastic and thermal properties of Ag-chalcopyrites ( $AgAlX_2$ :  $X = S, Se$ ), *Mater. Sci. Semicond. Process.* 26 (2014) 187–198.
- [22] P. Pichanusakorn, P. Bandaru, Nanostructured thermoelectrics, *Mater. Sci. Eng. R* 67 (2010) 19–63.
- [23] A. Charoenphakdee, K. Kurosaki, H. Muta, M. Uno, S. Yamanaka, Thermal conductivity of the ternary compounds:  $AgMT_2$  and  $AgM_5Te_8$  ( $M=Ga$  or  $In$ ), *Mater. Trans.* 50 (2009) 1603–1606.
- [24] D.C. Nguyen, S. Ito, Narrow band gap  $AgInTe_2$  solar cells fabricated by printing method, *Energy Sci. Technol.* 4 (2012) 1–5, 10.3968/j.est.1923847920120402.536.
- [25] A. Uzum, N. Takahashi, S. Ito, Narrow bandgap solar cells using  $AgInTe_2$ , in: 29th European Photovoltaic Solar Energy Conference and Exhibition, 22 – 26, September 2014, pp. 356–358, 10.4229/EUPVSEC20142014-1BV.7.75.
- [26] K.L. Chopra, P.D. Paulson, V. Dutta, Thin-film solar cells: an overview, *Prog. Photovol.* 12 (2004) 69–92.
- [27] M.K.S.B. Rafiq, N. Amin, H.F. Alharbi, M. Luqman, A. Ayob, Y.S. Alharthi, N.H. Alharthi, B. Bais, M. Akhtarruzzaman,  $WS_2$ : a new window layer material for solar cell application, *Sci. Rep.* 10 (2020) 7711.
- [28] D. Lilhare, A. Khare, Development of chalcogenide solar cells: importance of  $CdS$  window layer, *Opto-Electron. Rev.* 28 (2020) 43–63.
- [29] J. He, L. Wu, L. Feng, J. Zheng, J. Zhang, W. Li, B. Li, Y. Cai, Structural, electrical and optical properties of annealed  $Al/Sb$  multiayer films, *Sol. Energy Mater., Sol. Cell.* 95 (2011) 369–372.
- [30] K. Seeger, E. Schonherr, Microwave dielectric constant of aluminium antimonide, *Semicond. Sci. Technol.* 6 (1991) 301.
- [31] F.F. Yao, Z. Lei, L.H. Feng, J.Q. Zhang, W. Li, L.L. Wu, W. Cai, Y.P. Cai, J.G. Zheng, B. Li, Preparation of  $AlSb$  polycrystalline thin films by co-evaporation, *Chin. J. Semicond.* 27 (2006) 1578.
- [32] A. Hemani, D. Benmoussa, A. Nouri, H. Khachab, Effect of the FSF and BSF layers on the performances of the  $GaAs$  solar cell, *J. Ovonic Res.* 13 (2017) 307–314.
- [33] M.M.A. Moon, M.H. Ali, M.F. Rahman, A. Kuddus, J. Hossain, A.B.M. Ismail, Investigation of thin-film p- $BaSi_2/n-CdS$  heterostructure towards semiconducting silicide based high efficiency solar cell, *Phys. Scripta* 95 (2020), 035506.
- [34] K. Morita, Y. Inomata, T. Suemasu, Optical and electrical properties of semiconducting  $BaSi_2$  thin films on Si substrates grown by molecular beam epitaxy, *Thin Solid Films* 508 (2006) 363.
- [35] F.J. Zhao, Q. Xie, Q. Chen, C.H. Yang, First-principles calculations on the electronic structure and optical properties of  $BaSi_2$ , *Sci. China G* 52 (2009) 580–586.
- [36] K.O. Hara, Y. Nakagawa, T. Suemasu, N. Usami, Simple vacuum evaporation route to  $BaSi_2$  thin films for solar cell applications, *Procedia Eng.* 141 (2016) 27–31.
- [37] T. Deng, T. Sato, Z. Xu, R. Takabe, S. Yachi, Y. Yamashita, K. Toko, T. Suemasu, p- $BaSi_2/n-Si$  heterojunction solar cells on Si(001) with conversion efficiency approaching 10%: comparison with Si(111), *APEX* 11 (2018), 062301.
- [38] W. Du, R. Takabe, M. Baba, H. Takeuchi, K.O. Hara, K. Toko, N. Usami, T. Suemasu, Formation of  $BaSi_2$  heterojunction solar cells using transparent MoO<sub>x</sub> hole transport layers, *Appl. Phys. Lett.* 106 (2015), 122104.
- [39] D. Fomin, V. Dubov, K. Gal'kin, R. Batalov, V. Shustov, Formation and properties of crystalline  $BaSi_2$  thin films obtained by solid phase epitaxy on Si (111), in: *JJAP Conf. Proc.*, 5, 2017, 011203.
- [40] T. Yoneyama, A. Okada, M. Suzuno, T. Shibutami, K. Matsumaru, Formation of polycrystalline  $BaSi_2$  films by radio-frequency magnetron sputtering for thin-film solar cell applications, *Thin Solid Films* 534 (2013) 116–119.
- [41] T. Nakamura, T. Suemasu, K.-I. Takakura, F. Hasegawa, Investigation of the energy band structure of orthorhombic  $BaSi_2$  by optical and electrical measurements and theoretical calculations, *Appl. Phys. Lett.* 81 (2002) 1032–1034.
- [42] Q. Ma, H. Kyureghian, J. Banninga, N. Ianno, Thin-film  $AlSb$  for Use as a Photovoltaic Absorber Material, vol. 1670, Materials Research Society, Symposium E, 2014, p. 10, 02.
- [43] P. Tang, W. Wang, B. Li, L. Feng, G. Zeng, The properties of Zn-doped  $AlSb$  thin films prepared by pulsed laser deposition, *Coatings* 9 (2019) 136.
- [44] A. El-Korashy, M.A. Abdel-Rahim, H. El-Zahed, Optical absorption studies on  $AgInSe_2$  and  $AgInTe_2$  thin films, *Thin Solid Films* 338 (1999) 207–212.
- [45] N. Bensedidik, B. Belkacemi, F. Boukabrine, K. Aumeur, H. Mazari, A. Boumesjed, N. Benyahya, Z. Benamara, Numerical study of  $AgInTe_2$  solar cells using SCAPS, *Adv. Mater. Process. Technol.* (2020), <https://doi.org/10.1080/2374068X.2020.1833401>.
- [46] R. Vismara, O. Isabella, M. Zeman, Organometallic halide perovskite/barium di-silicide thin-film doublejunction solar cells Proc. SPIE, Photonics for Solar Energy Systems (2016), 98980J, VI 9898 (Brussels, Belgium, April 29).
- [47] L. Chen, H. Chen, Q. Deng, G. Wang, S. Wang, Numerical simulation of planar  $BaSi_2$  based Schottky junction solar cells toward high efficiency, *Solid State Electron.* 149 (2018) 46–51.
- [48] J. Hossain, M. Rahman, M.M.A. Moon, B.K. Mondal, M.F. Rahman, M.H.K. Rubel, Guidelines for a highly efficient  $Cu/n-Si$  heterojunction solar cell, *Eng. Res. Exp.* 2 (2020), 045019.
- [49] T. Ouslimane, L. Et-taya, L. Elmaimouni, A. Benami, Impact of absorber layer thickness, defect density, and operating temperature on the performance of  $MAPbI_3$  solar cells based on ZnO electron transporting material, *Heliyon* 7 (2021), e06379.
- [50] D.K. Shah, K.C. Devendra, M. Muddassir, M.S. Akhtar, C.Y. Kim, O.-B. Yang, A simulation approach for investigating the performances of cadmium telluride solar cells using doping concentrations, carrier lifetimes, thickness of layers, and band gaps, *Sol. Energy* 216 (2021) 259–265.
- [51] C.S. Jiang, M. Yang, Y. Zhou, B. To, S.U. Nanayakkara, J.M. Luther, W. Zhou, J.J. Berry, J. Lagemaat, N.P. Padture, K. Zhu, M.M. Al-Jassim, Carrier separation and transport in perovskite solar cells studied by nanometre-scale profiling of electrical potential, *Nat. Commun.* 6 (2015) 8397.
- [52] B.K. Mondal, S.K. Mostaque, J. Hossain, Theoretical insights into a high-efficiency  $Sb_2Se_3$ -based dual-heterojunction solar cell, *Heliyon* 8 (2022), e09120.
- [53] M.M.A. Moon, M.H. Ali, M.F. Rahman, J. Hossain, A.B.M. Ismail, Design and simulation of  $FeSi_2$ -based novel heterojunction solar cells for harnessing visible and near-infrared light, *Phys. Status Solidi A* 217 (2020), 1900921.
- [54] A. Kuddus, Ismail, A.B.M. Ismail, J. Hossain, Design of a highly efficient  $CdTe$ -based dual-heterojunction solar cell with 44% predicted efficiency, *Sol. Energy* 221 (2021) 488–501.
- [55] J. Hossain, Design and simulation of double-heterojunction solar cells based on Si and GaAs wafers, *J. Phys. Commun.* 5 (2021), 085008.
- [56] J. Hossain, B.K. Mondal, S.K. Mostaque, Design of a highly efficient  $FeS_2$ -based dual-heterojunction thin film solar cell, *Int. J. Green Energy* 14 (2022) 1531–1542.
- [57] J. Hossain, M.M.A. Moon, B.K. Mondal, M.A. Halim, Design guidelines for a highly efficient high-purity germanium (HPGe)-based double-heterojunction solar cell, *Opt. Laser. Technol.* 143 (2021), 107306.
- [58] Y.H. Khattak, F. Baig, H. Toura, S. Beg, B.M. Soucase, Efficiency enhancement of  $Cu_2BaSnS_4$  experimental thin-film solar cell by device modeling, *J. Mater. Sci.* 54 (2019) 14787–14796.
- [59] Faridah Ferdiansjah, K.T. Mularso, Analysis of back surface field (BSF) performance in P-type and N-type monocrystalline silicon wafer, in: E3S Web of Conferences 43, 2018, 01006.
- [60] S. Ahmed, A. Aktar, J. Hossain, A.B.M. Ismail, Enhancing the open circuit voltage of the SnS based heterojunction solar cell using NiO HTL, *Sol. Energy* 207 (2020) 693–702.

- [61] S.R.I. Biplab, M.H. Ali, M.M.A. Moon, M.F. Pervez, M.F. Rahman, J. Hossain, Performance enhancement of CIGS-based solar cells by incorporating an ultrathin BaSi<sub>2</sub> BSF layer, *J. Comput. Electron.* 19 (2019) 342–352.
- [62] B.K. Mondal, S.K. Mostaque, J. Hossain, Unraveling the effects of a GeSe BSF layer on the performance of a CuInSe<sub>2</sub> thin film solar cell: a computational analysis, *Optics Continuum* 2 (2023) 428–440.
- [63] L. Stolt, J. Hedström, J. Kessler, M. Ruckh, K.O. Velthaus, H.W. Schock, ZnO/CdS/CuInSe<sub>2</sub> thin-film solar cells with improved performance, *Appl. Phys. Lett.* 62 (6) (1998) 597.